

Article

# Xanthine Oxidase Inhibition and Anti-LDL Oxidation by Prenylated Isoflavones from *Flemingia philippinensis* Root

Jeong Yoon Kim <sup>1</sup>, Yan Wang <sup>2</sup> , Zuo Peng Li <sup>1</sup>, Aizhamal Baiseitova <sup>1</sup> , Yeong Jun Ban <sup>1</sup> and Ki Hun Park <sup>1,\*</sup>

<sup>1</sup> Division of Applied Life Science (BK21 Plus), IALS, Gyeongsang National University, Jinju 52828, Korea; foryou6633@gmail.com (J.Y.K.); dameng@126.com (Z.P.L.); aizhabaiseitova@gmail.com (A.B.); banyoung972@naver.com (Y.J.B.)

<sup>2</sup> College of Food and Biological Engineering, Qiqihar University, Qiqihar 161006, China; pitwang05@163.com

\* Correspondence: khpark@gnu.ac.kr; Tel.: +82-55-772-1965; Fax: +82-55-772-1969

Received: 15 June 2020; Accepted: 3 July 2020; Published: 6 July 2020



**Abstract:** Xanthine oxidase is a frontier enzyme to produce oxidants, which leads to inflammation in the blood. Prenylated isoflavones from *Flemingia philippinensis* were found to display potent inhibition against xanthine oxidase (XO). All isolates (1–9) inhibited XO enzyme with IC<sub>50</sub> ranging 7.8~36.4 μM. The most active isoflavones (2–5, IC<sub>50</sub> = 7.8~14.8 μM) have the structural feature of a catechol motif in B-ring. Inhibitory behaviors were disclosed as a mixed type I mode of inhibition with  $K_I < K_{IS}$ . Binding affinities to XO enzyme were evaluated. Fluorescence quenching effects agreed with inhibitory potencies (IC<sub>50</sub>s). The compounds (2–5) also showed potent anti-LDL oxidation effects in the thiobarbituric acid-reactive substances (TBARS) assay, the lag time of conjugated diene formation, relative electrophoretic mobility (REM), and fragmentation of apoB-100 on copper-mediated LDL oxidation. The compound 4 protected LDL oxidation with 0.7 μM in TBARS assay, which was 40-fold more active than genistein (IC<sub>50</sub> = 30.4 μM).

**Keywords:** *Flemingia philippinensis*; prenylated isoflavones; xanthine oxidase inhibition; anti-LDL oxidation

## 1. Introduction

Reactive oxygen species (ROS) have received important consideration due to their adjusted role in signaling during inflammation [1,2]. These oxidants produced commonly by NAD(P)H oxidase, nitric oxide (NO) synthase and xanthine oxidoreductase (XOR) as well as environmental factors such as stress, smoking, etc. [3,4]. In particular, the xanthine oxidase (XO, EC 1.17.3.2), one of two XOR interconvertible forms, is a crucial enzyme in the catabolism of purine, which oxidizes hypoxanthine into xanthine followed by xanthine transformation to uric acid [5,6]. Also, XO is a frontier enzyme to produce oxidants (ROS), such as superoxide anion (O<sub>2</sub><sup>•-</sup>) and hydrogen peroxide, because of its ability to transfer electron to molecular oxygen [7,8]. Endothelium-associated XO or XOR activity contributes to oxidative stress in blood vessels and inflammatory consequences arising from hypercholesterolemia and atherosclerosis [3,9]. Thus, controlling of XO excessive expression by its inhibitors—allopurinol and febuxostat—as the most widely prescribed commercial drugs, is important for human health, in particular, in regulation of vascular function [10]. However, they are often limited due to their inverse side effects, so the discoveries of new XO inhibitors are increasing.

On the other hand, there is a low-density lipoprotein (LDL) that is easily oxidized to oxLDL by ROS [11]. The oxLDL causes a form of cell accumulation and endothelial cell damages in the arterial intima, which finally promotes atherosclerosis [12,13]. The oxLDL stimulates monocytes to express cell surface adhesion molecules causing vascular oxidative damage [14]. Moreover, oxLDL and the level of its receptors have been certainly associated with various types of cancer [15]. A representative anti-LDL substance, probucol has been used as antihyperlipidemic drug [16]. Thus, XO inhibitors and anti-LDL substances can contribute to suppress the production of ROS and oxidative damage of intima [17]. In this research, we explored effective antioxidant substances blocking XO enzymes as well as LDL oxidation.

The merit of *Flemingia philippinensis* lies on its wide cultivation in the southern part of China for commercial purposes as nutraceutical and food ingredient. The roots part has been traditionally used for curing rheumatism arthropathy and for improving the density of bone [18]. A bright representative of a legume family, *F. philippinensis* produces secondary metabolites that mostly consist of prenylated isoflavones [19,20], but it also produces various polyphenol compounds, namely benzofurans [21], flavanones [22], and chromenones [23] in low quantities. The isolated metabolites or extracts reported have the anti-inflammatory [18], antiestrogenic [24], and immunosuppressive features [25]. The polyphenolic compounds also showed great potential for enzyme inhibitions to bacterial neuraminidase [20], protein tyrosine phosphatase 1B [26], and human neutrophil elastase [27]. Recently, antioxidative potentials were investigated up to the protection of DNA damage [28].

This work aims to investigate antioxidant potentials of prenylated isoflavones based on xanthine oxidase (XO) inhibition and anti-LDL oxidation. The chromatographic feature and relative abundance of prenylated isoflavones were illustrated by UPLC-ESI-TOF/MS. XO inhibition was characterized by using secondary plots of the Michaelis-Menten equation and fluorescence quenching experiments. Besides, the inhibition of LDL oxidation by all isolates were investigated by four different assay methods including relative electrophoretic mobility (REM).

## 2. Results and Discussion

### 2.1. Isolation of Isoflavones from *F. philippinensis*

*F. philippinensis* is a polyphenol-enriched plant. Since the plant belongs to the legume family, the major metabolites of the plant are derivatives of isoflavone. These isoflavones have not only biological functions as enzyme inhibitors, but also antitumor activities relating to ROS and angiogenesis [29,30]. In our study, most of the isoflavones were obtained by examining antioxidant power targeted against XO enzyme and LDL oxidation. As a result, nine isoflavones were isolated through repeated chromatographies according to the previous description [20].

The isolates (1–9) were elicited as genistein (1), auricularin (2), 6,8-diprenylorobol (3), 5,7,3',4'-tetrahydroxy-2',5'-di(3-methylbut-2-enyl)isoflavone (4), flemiphilippinin A (5), 5,7,3'-trihydroxy-2'-(3-methylbut-2-enyl)-4',5'-(3,3-dimethylpyrano)isoflavone (6), 8- $\gamma,\gamma$ -dimethylallylwighteone (7), osajin (8), and flemingsin (9) as shown in Figure 1. Their structures were elucidated by their spectroscopic data and comparing to those of previous reports [20,27]. Among the isolated compounds the most antioxidant, compound 4 had a molecular formula of C<sub>25</sub>H<sub>26</sub>O<sub>6</sub> as established by the [M + H]<sup>+</sup> ion at *m/z* 423.1806 (Calcd 422.1729) in the HR-ESI-MS analysis. The position of two prenyl appendages were clearly confirmed by HMBC correlations between H-1'' ( $\delta_{\text{H}} = 3.30$ ) and C-2' ( $\delta_{\text{C}} = 127.68$ ), H-1''' ( $\delta_{\text{H}} = 3.35$ ) and C-5' ( $\delta_{\text{C}} = 144.46$ ).

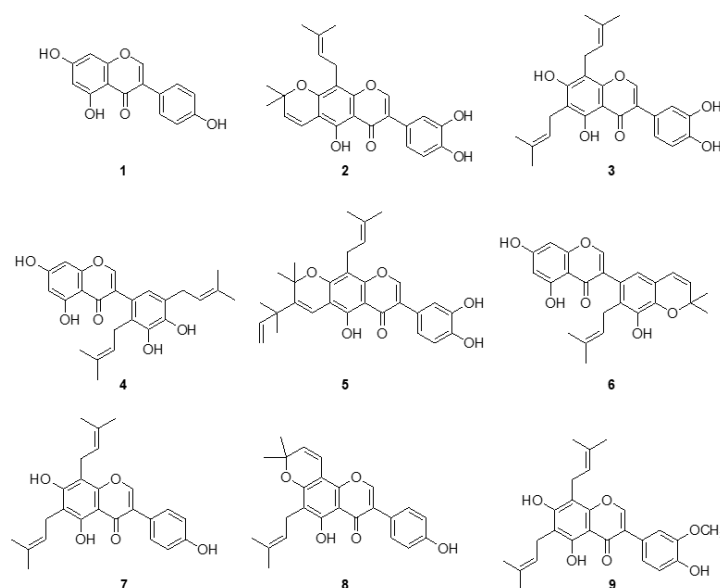


**Figure 1.** Chemical structures of the isolated isoflavones 1–9 from the root barks of *F. philippinensis*.

## 2.2. Inhibitory Effect of Isolated Isoflavones on Xanthine Oxidase (XO) Activity

XO is an important enzyme capable of producing oxidants like ROS [3]. The dysregulation of this enzyme may lead to oxidative stress accompanied by impaired vascular function and subsequent cardiovascular diseases [5,9]. The activity of XO was screened by procedure represented in the previous report, where stepwise oxidation of xanthine ( $\lambda_{\max} = 270$  nm) to uric acid ( $\lambda_{\max} = 295$  nm) was observed [31]. All isolates (1–9) inhibited XO with an  $IC_{50}$  range of 7.8–36.4  $\mu\text{M}$ . Dose-dependence of inhibitions was observed on all isolates as shown in Figure 2a. The most potent inhibitor 3 ( $IC_{50} = 7.8$   $\mu\text{M}$ ) showed a similar tendency with commercially available inhibitor, allopurinol (Table 1). The subtle changes in structures slightly affected the activity. The catechol motif in B ring was preferred over the corresponding product of C4-hydroxyl group; 3 ( $IC_{50} = 7.8$   $\mu\text{M}$ ) vs. 7 ( $IC_{50} = 16.9$   $\mu\text{M}$ ). The prenyl groups in resorcinol motif within A ring contributed to increasing the inhibitory potency: 1 ( $IC_{50} = 25.0$   $\mu\text{M}$ ) vs. 7 ( $IC_{50} = 16.9$   $\mu\text{M}$ ). The products (5 and 6) of oxidative cyclization of the alcohol group with a prenyl group tend to decrease activities to 14.8  $\mu\text{M}$  and 20.4  $\mu\text{M}$ , respectively. The reversibility of inhibitor to the enzyme was deduced with the plots derived from initial velocity versus enzyme amount in the different concentrations (0–12.5  $\mu\text{M}$ ) of compound 3 (Figure 2b). They showed a typical reversible type of inhibition where all of the straight lines passed through the origin. Other compounds were also reversible inhibitors to XO enzyme with a similar pattern of compound 3. The XO inhibitory behavior of prenylated isoflavones (2–9) was estimated using double-reciprocal plots (Figures S21–S23).

**Table 1.** Xanthine oxidase inhibitory effects of compounds 1–9 isolated from *F. philippinensis*.

Compounds	$IC_{50}$ <sup>a</sup> ( $\mu\text{M}$ )	Inhibition Mode ( $K_i$ <sup>b</sup> , $\mu\text{M}$ )	$K_I$ ( $\mu\text{M}$ )	$K_{IS}$ ( $\mu\text{M}$ )
1	25.0 $\pm$ 2.3	Competitive (11.5 $\pm$ 0.4)	NT <sup>c</sup>	NT
2	12.4 $\pm$ 0.8	Mixed type I (11.1 $\pm$ 0.5)	10.8	28.1
3	7.8 $\pm$ 0.6	Mixed type I (5.5 $\pm$ 0.3)	5.7	15.5
4	10.9 $\pm$ 0.4	Mixed type I (11.5 $\pm$ 0.3)	10.7	23.0
5	14.8 $\pm$ 1.2	Mixed type I (12.8 $\pm$ 0.2)	12.5	26.3
6	20.4 $\pm$ 0.2	Mixed type I (19.3 $\pm$ 0.8)	18.8	40.0
7	16.9 $\pm$ 0.4	Mixed type I (11.3 $\pm$ 0.3)	7.2	12.9
8	34.7 $\pm$ 1.6	Mixed type I (33.9 $\pm$ 1.3)	35.1	52.4
9	36.4 $\pm$ 0.5	Mixed type I (35.1 $\pm$ 0.9)	35.2	49.0
Allopurinol <sup>d</sup>	5.2 $\pm$ 0.1	NT	NT	NT

All compounds were examined in a set of experiments repeated three times; <sup>a</sup> Sample concentration which leads to 50% xanthine oxidase activity loss; <sup>b</sup> Values of inhibition constant; <sup>c</sup> NT is not tested; <sup>d</sup> Allopurinol was used as a positive control.

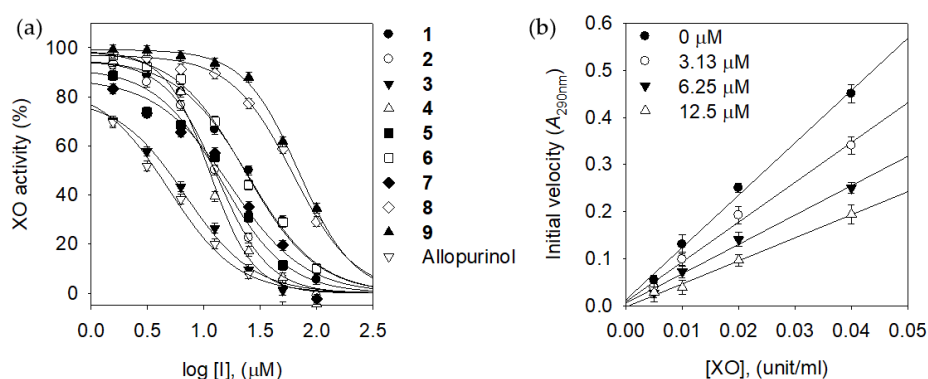


**Figure 2.** (a) Dose-dependent effects of the isolated compounds 1–9 and allopurinol on xanthine oxidase inhibition. (b) Determination of the reversible inhibitory mode of compound 3.

All estimated prenylated isoflavones were observed as mixed type inhibitors. As shown in Figure 3a, representative inhibitor 3 was elucidated as a typically mixed type inhibitor, because the common intercept in Lineweaver–Burk plots was on the left of the vertical axis and above the horizontal axis. It indicates that  $K_m$  was increased, whereas  $V_{max}$  decreased with the increasing concentration of 3. The secondary re-plots of the slope and intercept showed that  $K_i$  (5.7  $\mu\text{M}$ ) was much less than  $K_{IS}$  (15.5  $\mu\text{M}$ ). It is reasonable to conclude thus, compound 3 allowed as mixed type I, when inhibitor prefers free enzyme than substrate-enzyme complex. The  $K_i$  value of compound 3 was estimated to be 5.5  $\mu\text{M}$  by Dixon plots (Figure 3b). Meanwhile, genistein (1) was estimated as competitive inhibitor due to constant  $V_{max}$  and enhancing  $K_m$  by the increasing concentration of 1 (Figure 3c), agreed to the previous report [32]. Dixon plots (Figure 3d) of 1 determined the  $K_i$  value with 11.5  $\mu\text{M}$ .

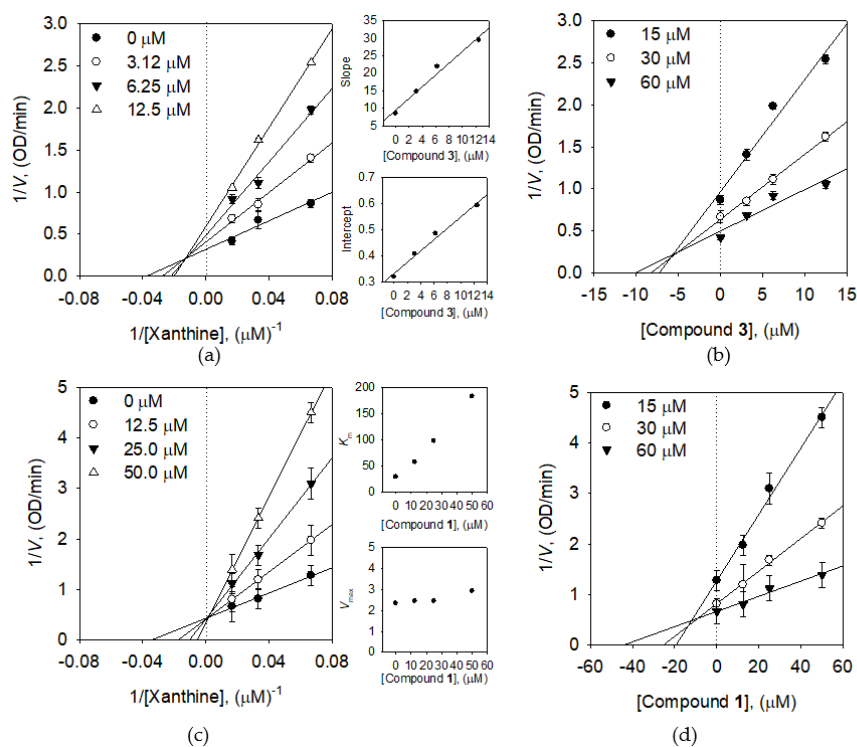


**Figure 3.** Enzymatic kinetics of compounds 3 and 1 using xanthine as a substrate. (a) Lineweaver–Burk plots of compound 3. (Inset) The secondary plots of the straight lines of slope and intercept versus the concentration of compound 3 throughout Equations (2)–(4) are shown. (b) Dixon plots of compound 3. (c) Lineweaver–Burk plots of compound 1 (Inset) Each curve provided tendencies for the Michaelis–Menten constant ( $K_m$ ) and maximal velocity ( $V_{max}$ ). (d) Dixon plots of compound 1.

### 2.3. Binding Affinity Between Xanthine Oxidase and Isolated Isoflavones

The XO enzyme has many numbers of fluorescent residues consist of 11 tryptophans, 34 tyrosines, and 68 phenylalanines according to [33] and Figure S26. Thus, the intrinsic fluorescence of XO enzyme is influenced by a function of the ligand concentration [32–34]. Fluorescence quenching (FS) effects were measured in the condition (excitation 290 nm, emission 300~400 nm) where there was no significant emission from any of the other components except enzyme. Results shown in Figure 4 demonstrates that FS intensities were reduced along with the inhibitor concentrations. Such wise, FS reduction tendencies had very close relations with inhibitory potencies ( $IC_{50}$  values). In particular, the compound **3** ( $IC_{50} = 7.8 \mu\text{M}$ ) showed more rapid FS reduction than compound **9** ( $IC_{50} = 36.4 \mu\text{M}$ ) and **1** ( $IC_{50} = 25.0 \mu\text{M}$ ). The binding affinity constant ( $K_{SV}$ ) which was calculated using the Stern–Volmer equation (equation (5)) could be ranked in the order of inhibitory potencies as follow: **3** ( $IC_{50} = 7.8$ ,  $K_{SV} = 1.2530$ ) > **5** ( $IC_{50} = 14.8$ ,  $K_{SV} = 0.5531$ ) > **1** ( $IC_{50} = 25.0$ ,  $K_{SV} = 0.1845$ ) > **9** ( $IC_{50} = 36.4 \mu\text{M}$ ,  $K_{SV} = 0.0930 \times 10^5 \text{ L}\cdot\text{mol}^{-1}$ ) given in Figure S24 and Table S1. A high correlation ( $R^2 = 0.9879$ ) between binding affinities ( $K_{SV}$ ) and inhibitory potencies ( $IC_{50}$ ) was observed (Figure 4d).

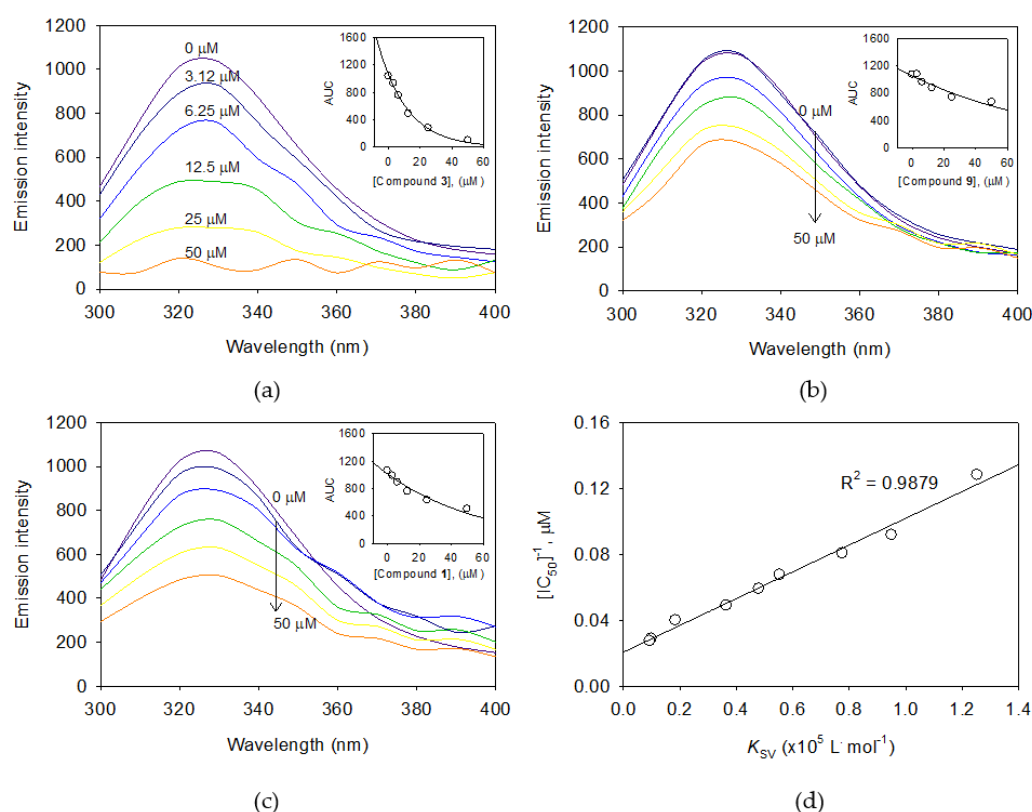


**Figure 4.** The fluorescence emission spectra of xanthine oxidase (XO) at different concentrations (0, 3.12, 6.25, 12.5, 25.0, and 50.0  $\mu\text{M}$ ) of (a) compound **3**, (b) compound **9**, and (c) compound **1**. (Inset) Normalized intensities of fluorescence for XO are shown for compounds **3**, **9**, and **1**, respectively. (d) The correlation between half-maximal inhibitory concentrations ( $IC_{50}$ ) values and Stern–Volmer constants ( $K_{SV}$ ) of compounds **1–9** is shown.

### 2.4. Protection Effects of Isoflavones on LDL Against Oxidative Damage

The isolated isoflavones (**1–9**) were evaluated *in vitro* for their antioxidant potential on  $\text{Cu}^{2+}$  induced LDL oxidation by using four different methods. All methods were carried out in the condition of human LDL (500  $\mu\text{g}/\text{mL}$ ) in the presence of 10  $\mu\text{M}$   $\text{Cu}^{2+}$  as an oxidation initiator according to the general procedure [35–38]. Firstly, in the thiobarbituric acid reactive substance (TBARS), all tested compounds exhibited antioxidant activities with a range of  $IC_{50}$  (0.7~30.4  $\mu\text{M}$ ) as shown in Table 2.

In particular, four prenylated isoflavones 2–5 showed a distinctive inhibition to LDL oxidation with  $IC_{50}$  values 2.4, 1.9, 0.7, and 2.7  $\mu\text{M}$ , respectively, which are 10–40 fold potent than genistein 1 ( $IC_{50} = 30.4$ ). The prenyl groups contributed to antioxidant potential as like genistein 1 ( $IC_{50} = 30.4$ ) vs. 6,8-diprenyl genistein 7 ( $IC_{50} = 14.6 \mu\text{M}$ ).

**Table 2.** Effects of isoflavones (1–9) from *F. philippinensis* on oxidized LDL induced by  $\text{Cu}^{2+}$ .

Compounds	$IC_{50}$ <sup>a</sup> ( $\mu\text{M}$ )	Inhibition Rate <sup>b</sup> (%)	Lag Time <sup>c</sup> (min)
1	$30.4 \pm 1.5$	20.3	80
2	$2.4 \pm 0.1$	95.9	>180
3	$1.9 \pm 0.3$	98.6	>180
4	$0.7 \pm 0.05$	100	>180
5	$2.8 \pm 0.5$	94.1	>180
6	$10.9 \pm 1.3$	48.8	152
7	$15.2 \pm 0.3$	38.7	124
8	$24.6 \pm 0.7$	25.4	108
9	$14.6 \pm 0.6$	40.3	128
Probucol <sup>d</sup>	$35.1 \pm 0.8$	16.4	83

All compounds were examined in triplicate. <sup>a</sup>  $IC_{50}$  values of isoflavones represent the concentration that caused 50% oxidation LDL by measurement of TBARS assay; <sup>b</sup> Inhibition rate was expressed at 10  $\mu\text{M}$  of isoflavones (1–9) concentration. <sup>c</sup> Lag time of conjugated diene formation by oxLDL at 10  $\mu\text{M}$  of isoflavones (1–9) concentration. <sup>d</sup> Probucol was used as a positive control.

Secondly, all isoflavones (1–9) were applied to the conjugated diene formation detecting at 234 nm for 180 min, of which lag time indicated the resistance of LDL oxidation. The control LDL (500  $\mu\text{g}/\text{mL}$ ) incubated with 10  $\mu\text{M}$   $\text{CuSO}_4$  had a lag time of 80 min, whereas antioxidants extended the lag time is proportional to their potential (Figure 5a). The lag times in Table 2 were associated with the results from TBARS assay as follows: 6 (152 min,  $IC_{50} = 10.9 \mu\text{M}$ ) > 9 (128 min, 14.6  $\mu\text{M}$ ) > 8 (108 min, 24.6  $\mu\text{M}$ ) > probucol (83 min, 35.1  $\mu\text{M}$ ). The four representative antioxidants 2–5 clearly showed to extend the lag time from 80 min to 180 min at 10  $\mu\text{M}$  concentrations. Dose-dependent of antioxidant concentration was demonstrated with the most active compound 4, of which lag time was extended to 120 min (0.3  $\mu\text{M}$ ), 160 min (0.6  $\mu\text{M}$ ), and 180 min (1.25  $\mu\text{M}$ ) as shown Figure 5b. The prenylated groups were proved to attribute LDL oxidation from genistein 1 (80 min) vs. its prenyl derivative 7 (124 min) at 10  $\mu\text{M}$  concentration (Figure 5b).

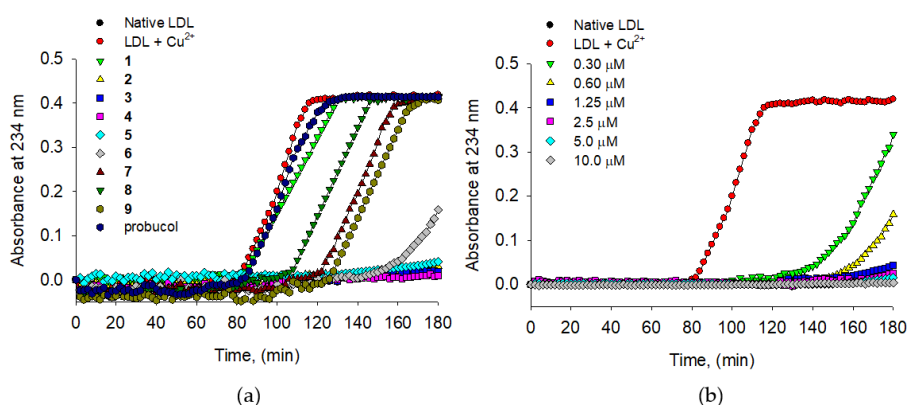


**Figure 5.** (a) Effects of isoflavones (1–9) on the generation of conjugated diene on  $\text{Cu}^{2+}$  induced LDL oxidation. (b) Dose-dependent effect of compound 4 on the generation of conjugated diene on  $\text{Cu}^{2+}$  induced LDL oxidation.

An oxidized LDL was also observed by the relative electrophoretic mobility (REM) assay method. The REM assay in Figure 6a was designed as follows: lane 1 (native LDL), lane 2 (oxidized LDL with 10  $\mu\text{M}$   $\text{CuSO}_4$ ), and lane 3–12 (native LDL and 10  $\mu\text{M}$  compounds with 10  $\mu\text{M}$   $\text{CuSO}_4$ ), which were

incubated for 16 h. The mobility of the LDL was clearly reduced by compounds **6**, **7**, and **9** that had 10~15  $\mu\text{M}$  of  $\text{IC}_{50}$ s in TBARS method. The most potent anti-LDL activities were observed on compounds **2–5**, which illustrated that REM results had a high correlation with TBARS (Figure 6a and Table 2). Figure 6b showed a dose-dependent activity of compound **4** at three different concentrations. Some selective compounds (**2–5**) were applied to ApoB-100, which is a major component of LDL and could be fragmented by ROS. The fragmentation of ApoB-100 was evaluated by the electrophoretic analysis on 4% polyacrylamide gel as shown in Figure 6c and Figure S25. The compounds **2–5** (lanes 4–7) protected the ApoB-100 fragmentation completely against copper-induced LDL oxidation at 2  $\mu\text{M}$  concentrations. The above four different methods proved that all isoflavones had antioxidant potentials to LDL oxidation. In particular, prenylated isoflavones (**2–5**) showed a distinctive inhibition of LDL oxidation at low concentrations.

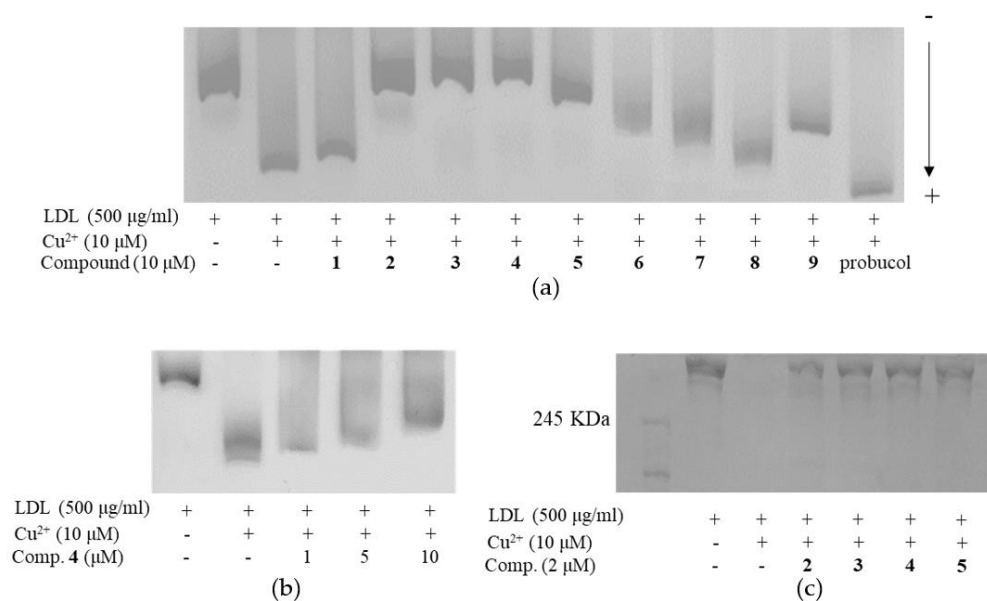


**Figure 6.** (a) Effect of isoflavones (**1–9**) on the  $\text{Cu}^{2+}$  mediated LDL oxidation by relative electrophoretic mobility (REM). (b) Dose-dependent effect of compound **4** against  $\text{Cu}^{2+}$  mediated LDL oxidation by REM. (c) Effects of isoflavones (**2–5**) on the ApoB-100 fragmentation.

### 2.5. Determination of Prenylated Isoflavones in the Plant by UPLC-Q-TOF-MS

MeOH extract of *F. philippinensis* was analyzed under optimized UPLC-Q-TOF-MS to estimate natural abundance of prenylated isoflavones in the plant. MS analysis and conditional optimization are crucial for obtaining fragment ions of the target compound. Nine isoflavones were deduced from the molecular formula of each chromatographic peak, fragment ion peak, the retention time of authentic compound, and reference [24,39] to the database (Table S2). The base peak intensity (BPI) positive ion chromatogram showed a complete chromatographic separation of major and minor peaks within 8 min as shown in Figure 7.

Peak 4 was identified as 5,7,3',4'-tetra-hydroxy-2',5'-di(3-methylbut-2-enyl)isoflavone (**4**) which yielded  $[\text{M} + \text{H}]^+$  ion at  $m/z$  423.1806 and a typical fragment ion  $[(\text{M} + \text{H}) - \text{C}_4\text{H}_8(\text{prenyl}) - \text{C}_4\text{H}_8(\text{prenyl})]^+$  at  $m/z$  311.0556. Peak 3 was structural isomer of peak 4 and determined as 6,8-diprenylorobol (**3**) with the same fragmentation pattern,  $[\text{M} + \text{H}]^+$  ion at  $m/z$  423.1806 and a fragment ion at  $m/z$  311.0557. Peaks 4 ( $t_R = 4.5$  min) and 3 ( $t_R = 5.2$  min) were distinguished by comparison of retention times of their authentic samples.

Peaks 6 (4.8 min) and 2 (5.8 min) were also structural isomers of each other. Peak 6 was found out as 5,7,3'-trihydroxy-2'-(3-methylbut-2-enyl)-4',5'-(3,3-dimethyl-pyrano)isoflavone (**6**) with an  $[\text{M} + \text{H}]^+$  ion at  $m/z$  421.1655 and a fragment ion at  $m/z$  365.1025. Peak 2 was identified as auriculasin (**2**) having an  $[\text{M} + \text{H}]^+$  ion at  $m/z$  421.1655 and a fragment ion at  $m/z$  365.1025.

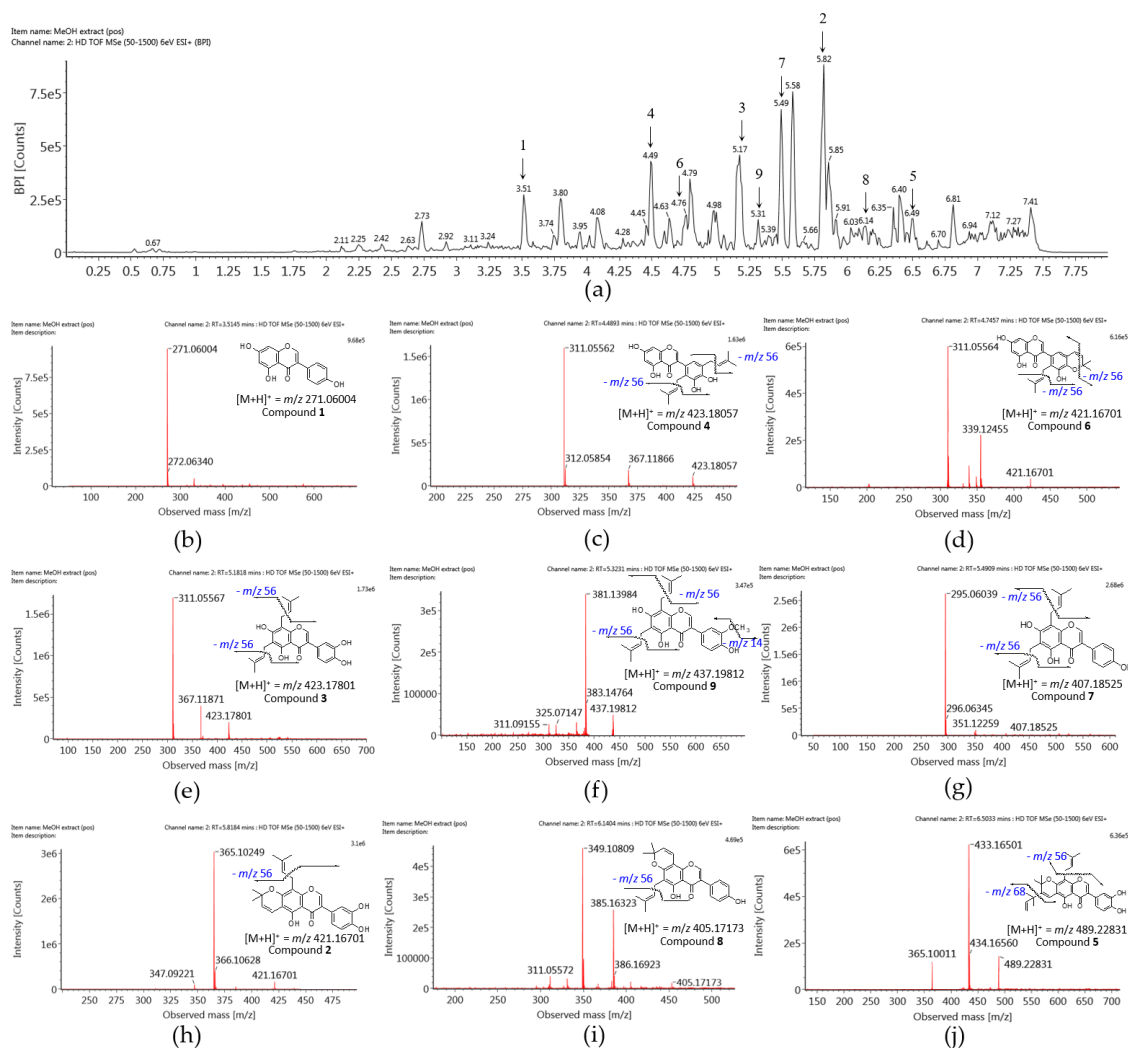


**Figure 7.** (a) The UPLC-ESI-TOF/MS chromatogram by base peak intensity (BPI) from the root barks of *F. philippinensis* methanol extract. Mass spectrum of nine isoflavones; (b) genistein (1); (c) 5,7,3',4'-tetra-*a*-hydroxy-2',5'-di(3-methylbut-2-enyl)isoflavone (4); (d) 5,7,3'-trihydroxy-2'-(3-methylbut-2-enyl)-4',5'-(3,3-dimethylpyrano)isoflavone (6); (e) 6,8-diprenylorobol (3); (f) flemingsin (9); (g) 8- $\gamma,\gamma$ -dimethyl-allylwighteone (7); (h) auricularin (2); (i) osajin (8); (j) flemiphilippinin A (5).

Peak 9 had an  $[M + H]^+$  ion at  $m/z$  437.1968 and a fragment ion  $[M + H - 56(\text{prenyl})]^+$  at  $m/z$  381.1398 to be flemingsin (9). Peak 7 had an  $[M + H]^+$  ion at  $m/z$  407.1853 and a fragment ion  $[M + H - 56 - 56]^+$  at  $m/z$  295.0604 to be 8- $\gamma,\gamma$ -dimethylallylwighteone (7). Peak 8 was identified as osajin (8) due to an  $[M + H]^+$  ion at  $m/z$  405.1706 and a fragment ion  $[M + H - 56]^+$  at  $m/z$  349.1081. Peak 5 was identified as flemiphilippinin A (5) due to an  $[M + H]^+$  ion at  $m/z$  489.2283, and fragment ions  $[M + H - 56]^+$  at  $m/z$  433.1650 and  $[M + H - 56 - 68]^+$  at  $m/z$  365.1001. These isoflavones (2–9) corresponded to the antioxidative effect in extract and were determined as predominant and/or moderate metabolites in *F. philippinensis*.

### 3. Materials and Methods

#### 3.1. Plant Materials and Chemicals

Root barks of *F. philippinensis* were gathered from a farm in Ninning, Guanxi province, China. The plant was confirmed with Voucher specimens (No. 530) by Dr. Yimin Zhao, Gaunxi Botanical Garden, China. It was cleaned, dried, and stored at a cool temperature ( $<18^\circ\text{C}$ ) in darkness. Methanol,

chloroform, butanol, *n*-hexane, sodium hydroxide (NaOH), and copper sulfate (CuSO<sub>4</sub>) were purchased from Duksan Co. (Gyeonggi-do, South Korea). Xanthine oxidase from bovine milk (EC 1.17.3.2), xanthine, allopurinol, sodium pyrophosphate, dimethyl sulfoxide (DMSO), probucol, thiobarbituric acid, trichloroacetic acid, and other used organic solvent were from Sigma Aldrich Co., (St. Louis, MO, USA). Low-density lipoprotein (LDL) was taken from Invitrogen (Thermo Fisher Scientific, Carlsbad, California, USA). ODS-C18 and Triart prep C18-S were from YMC Co., (Kyoto, Japan). Agarose, sodium dodecyl sulfate (SDS), *N,N,N',N'*-tetramethylethylenediamine (TEMED), coomassie brilliant blue R-250, ammonium persulfate (APS), and sample buffer were purchased from Bio-Rad (Hercules, CA, USA).

### 3.2. Instruments

The isoflavones (1–9) from *F. philippinensis* were isolated by using Forte/R 100 MPLC (YMC Co., Ltd., Kyoto, Japan). The identification of compound structures was made based on <sup>1</sup>H, <sup>13</sup>C, DEPT-90, 135, COSY, HMQC, and HMBC spectra (Bruker 500MHz NMR, Billerica, MA, USA). All the experiments measuring of absorption and fluorescence were performed on a multi-mode microplate reader SpectraMax M3 (Molecular Devices, San Jose, CA, USA). Measurement of REM and ApoB-100 fragmentations were conducted using the Mini-Electrophoresis system (TAESHINE Bioscience, Gyeonggi-do, South Korea) and SDS-PAGE (Bio-Rad, Hercules, CA, USA), respectively. High-resolution electrospray ionization mass spectra (HR-ESI-MS) were obtained from Acquity-LC and Vion-MS (Waters, Milford, CT, USA).

### 3.3. Extraction and Isolation of Isoflavones from *F. philippinensis*

The metabolites were isolated using a slight modification to the reported method [20]. Briefly, the dried root barks of *F. philippinensis* (0.5 kg) were extracted with MeOH (5 L × 3) to give a dark red extract (73 g, 14.6%). The extract was dissolved in water and fractionated by the increasing polarity of the solvent system from hexane, chloroform up to butanol. The chloroform fraction (2 g) was subjected to MPLC over ODS-C18 packed glass column (35 × 250 mm, 40 μm), eluted with the gradient solvent system from 10 to 100% MeOH to yield ten fractions (A–J). It was repeated 7 times to yield isoflavones rich fractions: C 1.3 g; D 1.6 g; E 0.9 g. The fraction C was eluted by the gradient solvent system (40–100% MeOH) in recycle HPLC with Triart Prep C18-S (250 × 4.6 mm, S-10 μm, 12 nm) to yield compounds 1 (9mg), 4 (24 mg), 6 (16 mg) and 3 (28 mg). The fraction D was rechromatographed using recycle HPLC over ODS-C18 column in recycling system and the fraction was eluted with 60% MeOH to give compounds 9 (15 mg), 7 (21 mg) and 2 (22 mg). The fraction E was chromatographed on reversed silica (250 g, 25 μm) by 50 % MeOH to yield compounds 8 (9 mg) and 5 (11 mg). The structural identification data of isolated compounds (1–9) was presented in the Supplementary Materials (Figures S1–S20). Spectroscopic data of selected compounds (2–5) were given below.

#### 3.3.1. Auriculasin (2)

UV (MeOH) λ<sub>max</sub> (log ε) 272 (3.54) nm; HR-ESI-MS 420.1582 [M]<sup>+</sup> (calcd for C<sub>25</sub>H<sub>24</sub>O<sub>6</sub> 420.1573); <sup>1</sup>H-NMR (500 MHz, CDCl<sub>3</sub>): δ 1.49 (H-5'' and 6''), 1.69 (H-4'''), 1.82 (H-5'''), 3.35 (H-1'''), 5.24 (H-2'''), 5.60 (H-2''), 6.70 (H-1''), 6.78 (H-6'), 6.99 (H-5'), 7.29 (H-2'), 7.86 (H-2), 12.93 (OH-5).

#### 3.3.2. 6,8-Diprenylorobol (3)

UV (MeOH) λ<sub>max</sub> (log ε) 260 (4.21), 280 (3.38) nm; HR-ESI-MS 422.1733 [M]<sup>+</sup> (calcd for C<sub>25</sub>H<sub>26</sub>O<sub>6</sub> 422.1729); <sup>1</sup>H-NMR (500 MHz, Acetone-*d*<sub>6</sub>): δ 1.77 (H-4'' and 4'''), 1.85 (H-5'' and 5'''), 3.47 (H-1''), 3.49 (H-1'''), 5.25 (H-2'' and 2'''), 6.75 (H-6'), 6.80 (H-5'), 6.97 (H-2'), 7.90 (H-2), 12.90 (OH-5).

### 3.3.3. 5,7,3',4'-Tetrahydroxy-2',5'-di(3-methylbut-2-enyl)isoflavone (4)

UV (MeOH)  $\lambda_{\max}$  (log  $\epsilon$ ) 260 (4.50), 276 (2.96) nm; HR-ESI-MS 422.1733 [M]<sup>+</sup> (calcd for C<sub>25</sub>H<sub>26</sub>O<sub>6</sub> 422.1729); <sup>1</sup>H-NMR (500 MHz, Acetone-*d*<sub>6</sub>),  $\delta$  1.45 (H-4''), 1.54 (H-5''), 1.71 (H-4''' and 5'''), 3.30 (H-1''), 3.36 (H-1'''), 5.08 (H-2''), 5.34 (H-2'''), 6.30 (H-6), 6.43 (H-8), 6.54 (H-6'), 7.89 (H-2), 13.01 (OH-5).

### 3.3.4. Flemiphilippinin A (5)

UV (MeOH)  $\lambda_{\max}$  (log  $\epsilon$ ) 270 (2.32) nm; HRESIMS 488.2210 [M]<sup>+</sup> (calcd for C<sub>30</sub>H<sub>32</sub>O<sub>6</sub> 488.2199); <sup>1</sup>H-NMR (500 MHz, CDCl<sub>3</sub>):  $\delta$  1.31 (H-4'''' and 5'''''), 1.45 (H-4'' and 5''), 1.60 (H-4'''), 1.72 (H-5'''), 3.27 (H-1'''), 5.02 (H-3'''''), 5.15 (H-2'''), 5.88 (H-2'''''), 6.65 (H-1''), 6.68 (H-6'), 6.75 (H-5'), 6.90 (H-2'), 7.81 (H-2), 12.82 (OH-5).

## 3.4. Measurements of Xanthine Oxidase Activity

Bovine milk xanthine oxidase (XO, EC 1.17.3.2) activity was measured following the previous procedures [34,40]. In this assay, the formation of uric acid was measured spectrophotometrically at 295 nm at 37 °C, as a result of the reaction between xanthine oxidase and xanthine as a substrate. For the enzyme assay protocol, the tested isoflavones (1–9) and allopurinol as a positive control were dissolved in dimethyl sulfoxide (DMSO), and further diluted in different concentrations, from 0 to 2 mM, diluting twice at each step. The reaction mixture containing 160  $\mu$ L of 200 mM sodium pyrophosphate/HCl (pH 7.5), 10  $\mu$ L of diluted isoflavone or allopurinol, 20  $\mu$ L of 300  $\mu$ M xanthine ( $K_m = 30 \mu$ M), and 10  $\mu$ L of 0.2 unit/mL bovine milk xanthine oxidase (final concentration: 0.01 unit/mL) was placed in clear bottom 96-well microplates and screened for 30 min every 30 s. The half-maximal inhibitory concentrations (IC<sub>50</sub>) were calculated according to the enzyme inhibition rate (%) derived from the change of uric acid formation in comparison with the concentration of inhibitors. The inhibition rate derived from the non-linear regression fitting to Equation (1).

$$\text{Inhibition rate (\%)} = 100 \times [(\text{rate of control reaction} - \text{rate of inhibitor reaction})/\text{rate of control reaction}] \quad (1)$$

### 3.5. Xanthine Oxidase Inhibition Kinetics

The inhibition mode and inhibitory constants were determined by Lineweaver–Burk and Dixon plots. For obtaining double reciprocal plots, was measured the reaction absorbance of the enzyme, inhibited by different concentrations of inhibitors, with three concentrations of xanthine (15, 30, and 60  $\mu$ M) at 295 nm and 37 °C. The corresponding kinetic parameters, namely the Michaelis-Menten constant ( $K_m$ ), maximal velocity ( $V_{\max}$ ), inhibitory constant ( $K_i$ ), and dissociation constant of a binding site for the inhibitor to either free enzyme or the enzyme-substrate complex ( $K_I$  and  $K_{IS}$ ) were determined by Equations (2)–(4) [40].

$$1/V = K_m/V_{\max} (1 + [I]/K_I) 1/S + 1/V_{\max} \quad (2)$$

$$\text{Slope} = K_m/K_I V_{\max} [I] + K_m/V_{\max} \quad (3)$$

$$\text{Intercept} = 1/K_{IS} V_{\max} [I] + 1/V_{\max} \quad (4)$$

### 3.6. Fluorescence Quenching Measurements

The binding affinity between xanthine oxidase and isolated isoflavones were measured by fluorescence quenching method [33]. For the fluorescence quenching experiments, the Trp intensities of xanthine oxidase were monitored wavelength of emission from 300 to 400 nm and excitation of 290 nm. The reaction mixture containing 180  $\mu$ L of 200 mM sodium pyrophosphate/HCl (pH 7.5), 10  $\mu$ L of isolated isoflavones diluted in DMSO (3.125, 6.25, 12.5, 25.0, and 50.0  $\mu$ M), and 10  $\mu$ L of 1 unit/mL xanthine oxidase was placed in black/flat bottom 96-well microplates. The fluorescence emission spectra were observed in the absence ( $F_0$ ) or presence ( $F$ ) of isoflavones as quenchers. The quenching

parameters such as the Stern–Volmer constant ( $K_{SV}$ ), binding constant ( $K_A$ ), and the number of binding sites ( $n$ ) were determined by the Equations (5) and (6) [41].

$$F_0 - F = 1 + K_{SV} [Q] \quad (5)$$

$$\text{Log} [(F_0 - F)/F] = \log K_A + n \log [Q]_f \quad (6)$$

### 3.7. Measurements of Thiobarbituric Acid Reactive Substances (TBARS)

Thiobarbituric acid reactive substances (TBARS) assay was carried out according to the previous method with minor modifications [38]. The absorbance of a product of a reaction between thiobarbituric acid (TBA) and malondialdehyde (MDA) was measured at 540 nm. First, 220  $\mu\text{L}$  of 500  $\mu\text{g}/\text{mL}$  LDL in a buffer (10 mM PBS, pH 7.4), 10  $\mu\text{L}$  of 10  $\mu\text{M}$  of  $\text{CuSO}_4$ , and 10  $\mu\text{L}$  of different concentrations from 0 to 3 mM of isoflavones or probucol as a positive control were mixed in 1.5 mL Eppendorf tube and incubated at 37  $^\circ\text{C}$  for 4 h. After incubation, 100  $\mu\text{L}$  of trichloroacetic acid (TCA) and 100  $\mu\text{L}$  of 0.67% thiobarbituric acid (TBA)/0.05 N NaOH were added to the reaction mixture and heated in the water bath at 100  $^\circ\text{C}$  for 15 min. After heating, the mixture was cooled on the ice and centrifuged for 15 min at 3000 rpm. The absorbance of supernatant was measured and the  $\text{IC}_{50}$  values were calculated from the inhibition rate derived from Equation (1).

### 3.8. Measurements of Formed Conjugated Dienes (CD)

The formation of conjugated dienes from oxLDL was assessed by the method [35]. The conjugated diene formation occurred in the clear bottom 96-well plate. The mixture of each well containing 230  $\mu\text{L}$  of 550  $\mu\text{g}/\text{mL}$  LDL in the buffer (10 mM PBS, pH 7.4) and 10  $\mu\text{L}$  of 250  $\mu\text{M}$   $\text{CuSO}_4$  (final concentration: 10  $\mu\text{M}$ ) in the presence or absence of isoflavones or probucol as a positive control (final concentration: 10  $\mu\text{M}$ ) were incubated at 37  $^\circ\text{C}$  for 4 h. Then, the reaction was screened at 234 nm for 180 min every 5 min, continuously, incubating in the SpectraMax M3 multi-mode microplate reader. In the observed absorbance spectra, the lag time of tested samples was obtained as the endpoint indicated in the lag phase.

### 3.9. Measurements of Relative Electrophoretic Mobility (REM) and ApoB Fragmentation

The relative electrophoretic mobility (REM) of native LDL and oxidized LDL induced by  $\text{Cu}^{2+}$  was performed according to the procedures of references [35,36]. Before the electrophoresis, the samples containing 10  $\mu\text{M}$  of  $\text{CuSO}_4$  and 10  $\mu\text{M}$  of nine isoflavones or probucol were treated into LDL (500  $\mu\text{g}/\text{mL}$ ), then incubated for 16 h at 37  $^\circ\text{C}$  in dark condition. The native LDL and pretreated LDL samples loaded onto 0.5% agarose gel in TAE buffer (40 mM Tris-acetate with 1 mM EDTA, pH 8.0) and electrophoresed for 50 min at 100 V. After the electrophoresis, the gel was fixed in 40% ethanol with 10% acetic acid for 30 min, stained with 0.15% coomassie brilliant blue R250, and LDL bands visualized by using the destaining solution (methanol:acetic acid:water, 3:2:15, *v/v*).

The anti-LDL oxidation activity of four isoflavones (2–5) having the highest ratio of migrating distance from oxidized LDL in REM experiments was confirmed by measuring up the fragmentation of ApoB-100, LDL particle, according to the procedure [37]. The ApoB-100 fragmentation was performed on 4% SDS-PAGE for 150 min at 60 V. For the fragmentation assay sample contained native LDL, copper ion oxidized LDL in the presence or absence four isoflavones (final concentration: 2  $\mu\text{M}$ ) mixed with sample buffer, consisted of 3% SDS, 10% glycerol, and 5% 2-mercaptoethanol. The pretreated samples were heated for 5 min at 95  $^\circ\text{C}$ . The heated samples were cooled on ice and loaded on the SDS-PAGE in the buffer. After electrophoresis, the gel was stained and destained by using the same procedure with REM.

### 3.10. UPLC-ESI-TOF-MS Analysis

Metabolites of the *F. philippinensis* root barks methanol extract were analyzed by using ultra performance liquid chromatography quadrupole time-of-flight mass spectrometry (UPLC-Q-TOF-MS) equipped with sample manager-FTN, binary solvent manager from Acquity UPLC, and high-resolution ion mobility mass detector from Vion IMS Q ToF. On the base peak intensity (BPI) chromatogram, peaks of metabolites were separated by performing on Acquity UPLC BEH C<sub>18</sub> column (2.1 mm × 100 mm, 1.7 μm; Waters) at 25 °C with gradient solvent system constituting the mobile phase A (0.1% formic acid in water) and B (acetonitrile). The linear gradient solvent system was as follows: 0–3 min, 50% B; 3–5 min, 70% B; 5–7 min, 90% B; 7–8 min, 100% B. The flow rate was 0.35 mL/min and the injection volume was 1 μL. The Q-TOF-MS was conducted in positive mode directly by passing to the ESI interface without splitting. The operating condition for mass analysis was 3 kV of capillary voltage, 40 V of sample cone voltage, 800 L/h of desolvation gas (Ar) flow, 30 L/h of cone gas (Ar) flow, desolvation temperature at 440 °C, and ion source temperature at 100 °C. The mass data collected by applying the energy (20–45 eV) was observed in the range from the mass-to-charge ratio 50 to 1500, with Leucine-enkephalin used as lock mass (566.2771 Da for positive mode) at the rate of 0.2 s/cycle. The assignment for the precursor and fragment ion patterns of the individual isoflavones (1–9) possessed by the methanol extract of *F. philippinensis* were assessed by the UniFi software (version 1.8.2.169, Waters) linked to databases (Chempidder, Metlin, and human metabolome).

### 3.11. Statistical Analysis

The triple repetition of all experiments proves the reliability of the results, which further verified in Sigma Plot (version 10.0, Systat Software, Inc., San Jose, CA, USA). Deviations from the values were considered significant at  $p < 0.05$ .

## 4. Conclusions

Xanthine oxidase (XO) is a key enzyme for producing oxidants (ROS), excessive amounts of which cause damage to cell structure such as like LDL oxidation. The prenylated isoflavones, major metabolites of *F. philippinensis*, were found to inhibit LDL oxidation as well as XO enzyme. The isoflavones had IC<sub>50</sub> of 7.8–36.4 μM against XO enzymes with mixed type I inhibitory behavior. We also proved that the inhibitory potency rose from the binding affinity to the enzyme by fluorescence quenching effect. The most potent XO inhibitors (2–5) were proven to have potent anti-LDL activities by four different methods including REM assay. A natural abundance of antioxidative isoflavones (2–9) was demonstrated by BPI chromatogram of UPLC-ESI-TOF-MS. Disclosed antioxidant potentials would contribute to increasing the value of the target plant as a functional food ingredient.

**Supplementary Materials:** The following are available online, Figure S1–S20: Structural information through 1D and 2D NMR of nine isoflavones (1–9), Figure S21–S23: Enzyme kinetics of isoflavones (1–9), Figure S24 and Table S1: Results of fluorescence quenching between XO and isoflavones, Figure S25: Effects of isoflavones (2–5) by measuring ApoB fragmentation at 1 and 2 μM, Table S2: UPLC-Q-TOF/MS analysis of isoflavones from *F. philippinensis*, Figure S26: Amino acids sequence of xanthine oxidase from bovine milk.

**Author Contributions:** J.Y.K. and A.B. screened xanthine oxidase inhibitory activity and LDL oxidation activity of isolated isoflavones. Y.W. and Z.P.L. isolated and identified isoflavones from *F. philippinensis*. Y.J.B. analyzes the individual metabolites using UPLC-Q-TOF/MS. K.H.P. designed overall research. All authors have read and agreed to the published version of the manuscript.

**Funding:** This work was done with research funds from the Ministry Education, Republic of Korea through the National Research Foundation (NRF) grant funded by the South Korea government (No. 2015R1A6A1A03031413 and No. 2018R1A2B6001753). The BK21 Plus program supported scholarships for all students.

**Conflicts of Interest:** The authors declare no conflict of interest.

## References

1. Hensley, K.; Robinson, K.A.; Gabbita, S.P.; Salsman, S.; Floyd, R.A. Reactive oxygen species, cell signaling, and cell injury. *Free Radic. Biol. Med.* **2000**, *28*, 1456–1462. [[CrossRef](#)]
2. Mittal, M.; Siddiqui, M.R.; Tran, K.; Reddy, S.P.; Malik, A.B. Reactive oxygen species in inflammation and tissue injury. *Antioxid. Redox Signal.* **2014**, *20*, 1126–1167. [[CrossRef](#)] [[PubMed](#)]
3. Battelli, M.G.; Polito, L.; Bolognesi, A. Xanthine oxidoreductase in atherosclerosis pathogenesis: Not only oxidative stress. *Atherosclerosis* **2014**, *237*, 562–567. [[CrossRef](#)] [[PubMed](#)]
4. Weseler, A.R.; Bast, A. Oxidative stress and vascular function: Implications for pharmacologic treatments. *Curr. Hypertens. Rep.* **2010**, *12*, 154–161. [[CrossRef](#)] [[PubMed](#)]
5. Battelli, M.G.; Bortolotti, M.; Polito, L.; Bolognesi, A. The role of xanthine oxidoreductase and uric acid in metabolic syndrome. *Biochim. Biophys. Acta-Mol. Basis Dis.* **2018**, *1864*, 2557–2565. [[CrossRef](#)] [[PubMed](#)]
6. Kanbay, M.; Jensen, T.; Solak, Y.; Le, M.; Roncal-Jimenez, C.; Rivard, C.; Lanaspa, M.A.; Nakagawa, T.; Johnson, R.J. Uric acid in metabolic syndrome: From an innocent bystander to a central player. *Eur. J. Intern. Med.* **2016**, *29*, 3–8. [[CrossRef](#)]
7. Cantu-Medellin, N.; Kelley, E.E. Xanthine oxidoreductase-catalyzed reduction of nitrite to nitric oxide: Insights regarding where, when and how. *Nitric Oxide-Biol. Chem.* **2013**, *34*, 19–26. [[CrossRef](#)]
8. Kelley, E.E.; Khoo, N.K.H.; Hundley, N.J.; Malik, U.Z.; Freeman, B.A.; Tarpey, M.M. Hydrogen peroxide is the major oxidant product of xanthine oxidase. *Free Radic. Biol. Med.* **2010**, *48*, 493–498. [[CrossRef](#)]
9. Cai, H.; Harrison, D.G. Endothelial dysfunction in cardiovascular diseases: The role of oxidant stress. *Circ. Res.* **2000**, *87*, 840–844. [[CrossRef](#)]
10. Luna, G.; Dolzhenko, A.V.; Mancera, R.L. Inhibitors of Xanthine Oxidase: Scaffold Diversity and Structure-Based Drug Design. *ChemMedChem.* **2019**, *14*, 714–743. [[CrossRef](#)]
11. Chen, K.; Thomas, S.R.; Keaney, J.F. Beyond LDL oxidation: ROS in vascular signal transduction. *Free Radic. Biol. Med.* **2003**, *35*, 117–132. [[CrossRef](#)]
12. Mundi, S.; Massaro, M.; Scoditti, E.; Carluccio, M.A.; Van Hinsbergh, V.W.M.; Iruela-Arispe, M.L.; De Caterina, R. Endothelial permeability, LDL deposition, and cardiovascular risk factors—A review. *Cardiovasc. Res.* **2018**, *114*, 35–52. [[CrossRef](#)] [[PubMed](#)]
13. Pirillo, A.; Norata, G.D.; Catapano, A.L. LOX-1, OxLDL, and atherosclerosis. *Mediat. Inflamm.* **2013**, *2013*, 152786. [[CrossRef](#)] [[PubMed](#)]
14. Khan, B.V.; Parthasarathy, S.S.; Alexander, R.W.; Medford, R.M. Modified Low Density Lipoprotein and Its Constituents Augment Cytokine-activated Vascular Cell Adhesion Molecule-1 Gene Expression in Human Vascular Endothelial Cells. *J. Clin. Investig.* **1995**, *95*, 1262–1270. [[CrossRef](#)]
15. Bitorina, A.V.; Oligschlaeger, Y.; Shiri-Sverdlov, R.; Theys, J. Low profile high value target: The role of OxLDL in cancer. *Biochim. Biophys. Acta-Mol. Cell Biol. Lipids* **2019**, *1864*, 158518. [[CrossRef](#)]
16. Yamamoto, A. A unique antilipidemic drug—Probucol. *J. Atheroscler. Thromb.* **2008**, *15*, 304–305. [[CrossRef](#)]
17. Marchio, P.; Guerra-Ojeda, S.; Vila, J.M.; Aldasoro, M.; Victor, V.M.; Mauricio, M.D. Targeting early atherosclerosis: A focus on oxidative stress and inflammation. *Oxid. Med. Cell. Longev.* **2019**, *2019*, 8563845. [[CrossRef](#)]
18. Sun, G.; Xing, C.; Zeng, L.; Huang, Y.; Sun, X.; Liu, Y. *Flemingia philippinensis* Flavonoids Relieve Bone Erosion and Inflammatory Mediators in CIA Mice by Downregulating NF- $\kappa$ B and MAPK Pathways. *Mediat. Inflamm.* **2019**, *2019*, 5790291. [[CrossRef](#)]
19. Li, H.; Yang, M.; Miao, J.; Ma, X. Prenylated isoflavones from *Flemingia philippinensis*. *Magn. Reson. Chem.* **2008**, *46*, 1203–1207. [[CrossRef](#)]
20. Wang, Y.; Curtis-Long, M.J.; Yuk, H.J.; Kim, D.W.; Tan, X.F.; Park, K.H. Bacterial neuraminidase inhibitory effects of prenylated isoflavones from roots of *Flemingia philippinensis*. *Bioorganic Med. Chem.* **2013**, *21*, 6398–6404. [[CrossRef](#)]
21. Li, H.; Zhai, F.; Yang, M.; Li, X.; Wang, P.; Ma, X. A New benzofuran derivative from *flemingia philippinensis* Merr. et Rolfe. *Molecules* **2012**, *17*, 7637–7644. [[CrossRef](#)] [[PubMed](#)]

22. Wang, Y.; Curtis-Long, M.J.; Lee, B.W.; Yuk, H.J.; Kim, D.W.; Tan, X.F.; Park, K.H. Inhibition of tyrosinase activity by polyphenol compounds from *Flemingia philippinensis* roots. *Bioorganic Med. Chem.* **2014**, *22*, 1115–1120. [[CrossRef](#)]
23. Wang, Y.; Kim, J.Y.; Song, Y.H.; Li, Z.P.; Yoon, S.H.; Uddin, Z.; Ban, Y.J.; Lee, K.W.; Park, K.H. Highly potent bacterial neuraminidase inhibitors, chromenone derivatives from *Flemingia philippinensis*. *Int. J. Biol. Macromol.* **2019**, *128*, 149–157. [[CrossRef](#)] [[PubMed](#)]
24. Sun, F.; Li, Q.; Xu, J. Chemical Composition of Roots *Flemingia philippinensis* and Their Inhibitory Kinetics on Aromatase. *Chem. Biodivers.* **2017**, *14*, e1600193. [[CrossRef](#)] [[PubMed](#)]
25. Li, L.; Deng, X.; Zhang, L.; Shu, P.; Qin, M. A new coumestan with immunosuppressive activities from *Flemingia philippinensis*. *Fitoterapia* **2011**, *82*, 615–619. [[CrossRef](#)]
26. Wang, Y.; Yuk, H.J.; Kim, J.Y.; Kim, D.W.; Song, Y.H.; Tan, X.F.; Curtis-Long, M.J.; Park, K.H. Novel chromenedione derivatives displaying inhibition of protein tyrosine phosphatase 1B (PTP1B) from *Flemingia philippinensis*. *Bioorganic Med. Chem. Lett.* **2016**, *26*, 318–321. [[CrossRef](#)]
27. Kim, J.Y.; Wang, Y.; Uddin, Z.; Song, Y.H.; Li, Z.P.; Jenis, J.; Park, K.H. Competitive neutrophil elastase inhibitory isoflavones from the roots of *Flemingia philippinensis*. *Bioorganic Chem.* **2018**, *78*, 249–257. [[CrossRef](#)]
28. Kim, J.Y.; Wang, Y.; Song, Y.H.; Uddin, Z.; Li, Z.P.; Ban, Y.J.; Park, K.H. Antioxidant activities of phenolic metabolites from *Flemingia philippinensis* Merr. et Rolfe and their application to DNA damage protection. *Molecules* **2018**, *23*, 816. [[CrossRef](#)]
29. Cho, H.D.; Moon, K.D.; Park, K.H.; Lee, Y.S.; Seo, K.I. Effects of auriculasin on vascular endothelial growth factor (VEGF)-induced angiogenesis via regulation of VEGF receptor 2 signaling pathways in vitro and in vivo. *Food Chem. Toxicol.* **2018**, *121*, 612–621. [[CrossRef](#)]
30. Cho, H.D.; Lee, J.H.; Moon, K.D.; Park, K.H.; Lee, M.K.; Seo, K.I. Auriculasin-induced ROS causes prostate cancer cell death via induction of apoptosis. *Food Chem. Toxicol.* **2018**, *111*, 660–669. [[CrossRef](#)]
31. Priest, D.G.; Fisher, J.R. Substrate Activation with a Xanthine Oxidase Reaction: An Alternative to Dismutation as an Explanation in the Chicken Liver System. *Eur. J. Biochem.* **1969**, *10*, 439–444. [[CrossRef](#)]
32. Lin, S.; Zhang, G.; Pan, J.; Gong, D. Deciphering the inhibitory mechanism of genistein on xanthine oxidase in vitro. *J. Photochem. Photobiol. B Biol.* **2015**, *153*, 463–472. [[CrossRef](#)]
33. Yan, J.; Zhang, G.; Hu, Y.; Ma, Y. Effect of luteolin on xanthine oxidase: Inhibition kinetics and interaction mechanism merging with docking simulation. *Food Chem.* **2013**, *141*, 3766–3773. [[CrossRef](#)]
34. Tang, H.; Zhao, D. Investigation of the interaction between salvianolic acid C and xanthine oxidase: Insights from experimental studies merging with molecular docking methods. *Bioorganic Chem.* **2019**, *88*, 102981. [[CrossRef](#)]
35. Kim, J.Y.; Lee, J.W.; Lee, J.S.; Jang, D.S.; Shim, S.H. Inhibitory effects of compounds isolated from roots of *Cynanchum wilfordii* on oxidation and glycation of human low-density lipoprotein (LDL). *J. Funct. Foods* **2019**, *59*, 281–290. [[CrossRef](#)]
36. Jin, H.L.; Byong, W.L.; Jin, H.K.; Jeong, T.S.; Mim, J.K.; Woo, S.L.; Ki, H.P. LDL-antioxidant pterocarpans from roots of *Glycine max* (L) Merr. *J. Agric. Food Chem.* **2006**, *54*, 2057–2063.
37. Lin, C.Y.; Chen, P.N.; Hsieh, Y.S.; Chu, S.C. Koelreuteria formosana extract impedes in vitro human LDL and prevents oxidised LDL-induced apoptosis in human umbilical vein endothelial cells. *Food Chem.* **2014**, *146*, 299–307. [[CrossRef](#)]
38. Nagappan, H.; Pee, P.P.; Kee, S.H.Y.; Ow, J.T.; Yan, S.W.; Chew, L.Y.; Kong, K.W. Malaysian brown seaweeds *Sargassum siliquosum* and *Sargassum polycystum*: Low density lipoprotein (LDL) oxidation, angiotensin converting enzyme (ACE),  $\alpha$ -amylase, and  $\alpha$ -glucosidase inhibition activities. *Food Res. Int.* **2017**, *99*, 950–958. [[CrossRef](#)]
39. Xu, M.J.; Wu, B.; Ding, T.; Chu, J.H.; Li, C.Y.; Zhang, J.; Wu, T.; Wu, J.; Liu, S.J.; Liu, S.L.; et al. Simultaneous characterization of prenylated flavonoids and isoflavonoids in *Psoralea corylifolia* L. by liquid chromatography with diode-array detection and quadrupole time-of-flight mass spectrometry. *Rapid Commun. Mass Spectrom.* **2012**, *26*, 2343–2358. [[CrossRef](#)]
40. Kim, D.W.; Curtis-Long, M.J.; Yuk, H.J.; Wang, Y.; Song, Y.H.; Jeong, S.H.; Park, K.H. Quantitative analysis of phenolic metabolites from different parts of *Angelica keiskei* by HPLC-ESI MS/MS and their xanthine oxidase inhibition. *Food Chem.* **2014**, *153*, 20–27. [[CrossRef](#)]

41. Boaz, H.; Rollefson, G.K. The Quenching of Fluorescence. Deviations from the Stern-Volmer Law. *J. Am. Chem. Soc.* **1950**, *72*, 3435–3443. [[CrossRef](#)]

**Sample Availability:** Samples of the compounds 1–9 are available from the authors.



© 2020 by the authors. Licensee MDPI, Basel, Switzerland. This article is an open access article distributed under the terms and conditions of the Creative Commons Attribution (CC BY) license (<http://creativecommons.org/licenses/by/4.0/>).